Flow and acoustic fields of Reynolds number 10^5, subsonic jets with tripped exit boundary layers

Christophe Bogey[*], **Olivier Marsden**[†] and **Christophe Bailly**[‡]

Laboratoire de Mécanique des Fluides et d'Acoustique

UMR CNRS 5509, Ecole Centrale de Lyon

69134 Ecully, France

Compressible Large-Eddy Simulations of five isothermal round jets at a Mach number of 0.9 and a diameter-based Reynolds number of 10^5 originating from a pipe are reported, to examine the feasibility of computing the flow and acoustic fields of initially nominally turbulent jets. In the pipe the boundary layers are tripped in order to obtain at the exit section laminar mean velocity profiles of momentum thickness $\delta_\theta = 0.018$ times the jet radius, yielding a Reynolds number $\mathrm{Re}_\theta = 900$, as well as peak turbulent intensities around 9% of the jet velocity. Two methods of boundary-layer tripping, and four grids containing from 50 to 252 million points, are considered. The results are found to vary negligibly with the tripping procedure, but appreciably with the grid resolution. A high azimuthal resolution appears in particular necessary to simulate the initial shear-layer development properly. For the present tripped jet, $n_\theta = 256$ points in the azimuth are for instance insufficient, which has led us to specify $n_\theta = 1024$ points to reach a high level of confidence in the numerical solutions. A fine discretization of the mixing layers also seems to be required from the nozzle exit to the end of the potential core to get jet features similar to those measured at high Reynolds numbers.

I. Introduction

The importance of the initial conditions on free shear layers and jets is now well recognized. From the pionnering works by Batt[1] and Hill *et al.*,[2] it has been shown by Gutmark & Ho[3] and Raman *et al.*[4] for instance that minute variations in the nozzle-exit conditions of initially laminar jets are able to cause significant changes in the downstream flow development. The effects of exit conditions have also been found to be spectacularly significant on transitional jets. These jets, which are those at moderate Reynolds numbers around 10^5 typically considered using laboratory facilities, are indeed initially neither fully laminar nor fully turbulent. As discussed by Crighton,[5] Hussain[6] and Zaman,[7] among others, their turbulent and noise features therefore depend strongly on whether their nozzle-exit boundary layers contain low or high levels of velocity disturbances, *i.e.* whether they are nominally laminar (or weakly disturbed) or nominally turbulent (or highly disturbed).

The effects of the initial fluctuation levels on free shear flows have usually been investigated experimentally by installing additional devices inside the jet nozzle to trip the boundary layers, thus generating exit turbulent conditions for jets whose natural initial state would be laminar. This enables to vary the exit turbulence levels for jets at fixed Reynolds numbers, and is easy to implement even if the trip parameters may need to be determined by trial and error until the outlet conditions are satisfactory. The trip devices themselves can be of various kinds. Rough strips,[2,7–11] rings,[4,12–18] or round wires[1,19,20] mounted at the nozzle inner wall, grids[4] or screens[4,21,22] in the nozzle flow, or pipe extensions[13,14,23–25] have for example been successfully applied. In most cases they have moreover been used for jets at moderate diameter-based Reynolds numbers over the range $5 \times 10^4 \leq \mathrm{Re}_D \leq 5 \times 10^5$, characterized by initial shear layers of momentum thicknesses δ_θ

[*]CNRS Research Scientist, AIAA Member, christophe.bogey@ec-lyon.fr

[†]Assistant Professor at Ecole Centrale de Lyon, AIAA Member, olivier.marsden@ec-lyon.fr

[‡]Professor at Ecole Centrale de Lyon & Institut Universitaire de France, Senior AIAA Member, christophe.bailly@ec-lyon.fr

yielding Reynolds numbers Re_θ between 200 and 4000. To mention for instance the jet conditions in two sets of experiments, the Reynolds numbers were $\mathrm{Re}_D = 1.4 \times 10^5$ and $\mathrm{Re}_\theta = 700$ in the tripped round jet of Bridges & Hussain,[11] and they were between $10^5 \leq \mathrm{Re}_D \leq 2.5 \times 10^5$, and between $900 \leq \mathrm{Re}_\theta \leq 2250$ in the nominally turbulent jets of Zaman.[7,10]

In numerical simulations of jets, similar issues related to the influence of initial turbulence levels on the physical relevance of results have to be carefully taken into account. Because of the restrictions in terms of computational resources, and despite rapid progress in the field over the last decade,[26–28] this led us in particular to deal usually with low-Reynolds-number jets[29,30] or with initially laminar jets at moderate Reynolds numbers forced by disturbances of low magnitude.[31–34] Some attempts were made by Bogey *et al.*[35] and by Uzun & Hussaini[36] to compute initially turbulent jets. However the former simulation was unfortunately under-resolved, whereas the latter was performed on a grid discretizing finely the upstream boundary layers, but whose spatial extent was limited to 4.5 diameters downstream of the nozzle exit. Strong vortex pairing noise was also observed rather unexpectedly in the jet at $\mathrm{Re}_D = 10^5$ studied by Uzun & Hussaini.[36] It can be emphasized that the simulation of initially fully turbulent jets at Reynolds numbers $\mathrm{Re}_D \geq 10^5$ is still a real challenge. A very large number of grid points is indeed required both for the turbulent boundary layers inside the nozzle, and for the jet flow field developing outside, which should at least include the first 15 diameters downstream of the exit section. To bypass this difficulty, following the same approach as in experiments, we decided to perform simulations of jets whose boundary layers are tripped inside the nozzle to create highly disturbed, but not fully turbulent, nozzle-exit conditions.

In the present work, initially nominally turbulent subsonic round jets at Mach number 0.9 and Reynolds number $\mathrm{Re}_D = 10^5$ are therefore calculated by compressible Large-Eddy Simulations based on relaxation filtering (LES-RF) using low-dissipation and low-dispersion schemes. Inside a pipe nozzle, the jet boundary layers are tripped by the addition of random velocity disturbances to specify in all cases the same exit conditions as those measured in the tripped jets of Zaman.[7,10] The trip parameters are consequently adjusted so that the mean velocity profiles at the nozzle exit roughly correspond to a laminar Blasius profile of momentum thickness $\delta_\theta = 0.018$ times the pipe radius, and that the peak turbulence intensities are around 9% of the jet velocity. The main objective in this work is to investigate the feasibility of accurately computing nominally turbulent jets, and then to establish some requirements for obtaining trustworthy numerical solutions for these flows. With this aim in view, two different methods of boundary-layer tripping, and four meshes containing from 50 to 252 million points are used. The effects of the trip procedure and of the grid resolution on the shear layer transition, on the jet development as well as on the jet far-field noise determined by the LES will thus be described in detail.

The paper is organized as follows. In section II, the parameters of the jet LES and of the extrapolation of the LES near field to the far field, including numerical algorithm, computational grids and times, are documented. The initial conditions of the jets, as well as the flow conditions at the pipe exit, are also reported. The shear-layer developments and jet flow fields obtained in the different simulations are presented in section III, whereas the jet near and far acoustic fields are shown in section IV. Concluding remarks are provided in section V.

II. Simulation parameters

A. Jet definition

Five circular isothermal jets, hereafter referred to as Jetv9noise256, Jetv9ring256, Jetv9ring256drdz, Jetv9-ring512 and Jetv9ring1024dz depending on the boundary-layer tripping and grid used, are computed by Large-Eddy Simulation. They are at Mach number $\mathrm{M} = u_j/c_a = 0.9$ and at Reynolds number $\mathrm{Re}_D = u_j D/\nu = 10^5$, and originate from a pipe nozzle of radius r_0 and length $2r_0$ (u_j is the jet inflow velocity, c_a is the speed of sound in the ambient medium, $D = 2r_0$ is the nozzle diameter, and ν is the kinematic molecular viscosity). The ambient temperature and pressure are 293 K and 10^5 Pa. At the exit section of the nozzle at $z = 0$, the width of the nozzle lip is $0.053r_0$. At the pipe inlet at $z = -2r_0$, laminar Blasius boundary layers of thickness $\delta = 0.15r_0$, or equally of momentum thickness $\delta_\theta = 0.018r_0$, are imposed. The profiles of axial velocity u_z are more precisely given by a polynomial approximation of the Blasius profile. In addition, radial and azimuthal velocities are initially set to zero, pressure is kept constant at its ambient value, and the temperature is determined by a Crocco-Busemann relation.

To specify nozzle-exit conditions as close as possible to those in the nominally turbulent jets of Zaman,[7,10] the boundary layers are tripped inside the pipe at $z = -r_0$ as in Zaman's experiments. The tripping procedure

consists in simply adding random velocity fluctuations in the boundary layer. These fluctuations are fully random both in time and in space in Jetv9noise256, whereas they are based on vortical disturbances[31,35] decorrelated in the azimuthal direction in the four other jets, as shown in table 1. The tripping magnitudes have been empirically chosen to obtain, at the nozzle exit of the five jets, turbulence intensities around 9% of the jet velocity as well as mean-velocity profiles very similar to the laminar profiles of momentum thickness $\delta_\theta = 0.018 r_0$ imposed at the pipe inlet, which will be illustrated later in section II.C. It is indeed possible to find at the nozzle-exit section of tripped jets high levels of velocity fluctuations together with laminar velocity profiles, as clearly evidenced in the experimental works of Hussain and Zedan[9] for instance.

Table 1. Boundary-layer tripping in the simulations by adding fully random (*noise*), or vortical (*ring*), velocity disturbances in the pipe nozzle.

simulation	tripping
Jetv9noise256	*noise*
Jetv9ring256, Jetv9ring256drdz, Jetv9ring512, Jetv9ring1024dz	*ring*

B. LES procedure and parameters

The numerical methodology is identical to that used for recent simulations of initially laminar jets.[34] The LES are performed using a solver of the three-dimensional filtered compressible Navier-Stokes equations developed in cylindrical coordinates (r, θ, z) using low-dissipation and low-dispersion finite-difference schemes. The axis singularity is taken into account by the method proposed by Mohseni and Colonius.[37] Fourth-order eleven-point centered finite differences are used for spatial discretization, and a second-order six-stage low-storage Runge-Kutta algorithm is implemented for time integration.[38] To circumvent the severe time-step restriction induced by the cylindrical coordinates, the derivatives in the azimuthal direction around the axis are calculated using every n-th grid point, from $n = 2$ up to $n = 32$ or $n = 64$ near the centerline, depending on the azimuthal resolution. To remove grid-to-grid oscillations, a sixth-order eleven-point centered filtering designed to damp only the shortest waves discretized[39] is applied every time step to the flow variables. The discretization at the boundaries is taken into account by non-centered finite differences and filters with properties optimized in the Fourier space.[34,40] The filtering is also employed to dissipate subgrid-scale energy without significantly affecting the scales resolved accurately.[41] This LES approach was developed to avoid artificially decreasing the effective flow Reynolds number, which might be the case using eddy-viscosity subgrid models.[42] More details on this approach based on relaxation filtering, which can be referred to as LES-RF, are available in a paper.[43] Finally, in order to compute the radiated noise directly, non-reflective boundary conditions[44,45] are specified, with the addition of a sponge zone at the outflow. These non-reflective conditions are also applied at the pipe inlet. In this way, acoustic resonance inside the nozzle is unlikely, which will be supported by velocity spectra in section II.C.

Some parameters of the grids used for the five jet LES, containing from 50 up to 252 million points, are provided in table 2. In Jetv9noise256 and Jetv9ring256, the azimuth is discretized by $n_\theta = 256$ points, yielding $r_0 \Delta\theta = 0.0245 r_0$, while the mesh spacings at the pipe lip are $\Delta r = 0.0072 r_0$ and $\Delta z = 0.0145 r_0$ of the jet radius. In Jetv9ring256drdz, $n_\theta = 256$ is kept in the azimuth, but the mesh resolutions in the radial and the axial directions are twice as fine as previously at the nozzle lip. In Jetv9ring512, $n_\theta = 512$ points are then specified in the azimuthal direction, while using the radial and axial discretizations of Jetv9noise256 and

Table 2. Simulation parameters: numbers of grid points (n_r, n_θ, n_z), mesh spacings $(\Delta r, \Delta\theta, \Delta z)$, axial extend L_z of the physical domain in the axial direction, number of time steps n_t, and time duration T.

simulation	$n_r \times n_\theta \times n_z$	$\Delta r(r = r_0)$	$r_0 \Delta\theta$	$\Delta z(z = 0)$	L_z	n_t	$T u_j / r_0$
Jetv9noise256	$256 \times 256 \times 768$	$0.0072 r_0$	$0.0245 r_0$	$0.0145 r_0$	$32.5 r_0$	$81,000$	475
Jetv9ring256	$256 \times 256 \times 768$	$0.0072 r_0$	$0.0245 r_0$	$0.0145 r_0$	$32.5 r_0$	$81,000$	475
Jetv9ring256drdz	$290 \times 256 \times 992$	$0.0036 r_0$	$0.0245 r_0$	$0.0072 r_0$	$32.5 r_0$	$81,000$	475
Jetv9ring512	$256 \times 512 \times 654$	$0.0072 r_0$	$0.0123 r_0$	$0.0145 r_0$	$25 r_0$	$110,000$	325
Jetv9ring1024dz	$256 \times 1024 \times 962$	$0.0072 r_0$	$0.0061 r_0$	$0.0072 r_0$	$25 r_0$	$95,600$	437.5

Jetv9ring256. Given the results obtained from these first four cases, a fifth configuration, Jetv9ring1024dz, has been studied using a grid characterized by $n_\theta = 1024$ points in the azimuth, giving $r_0\Delta\theta = 0.0061r_0$, and by $\Delta r = \Delta z = 0.0072r_0$ at the nozzle lip. The physical domains, that are found upstream of eighty-point sponge zones applied at the outflow, extend axially up to $z = 32.5r_0$ in the first three jets, but up to $z = 25r_0$ in the two other jets computed using finer azimuthal resolutions. They also extend radially up to $r = 11r_0$ in all cases.

In the radial direction, the discretizations in the four simulations using $n_r = 256$ points, namely Jetv9-noise256, Jetv9ring256, Jetv9ring512 and Jetv9ring1024dz are the same. The radial mesh spacings Δr in these LES are represented in figure 1 from $r = 0$ to $r = 3r_0$, normalized by the jet radius r_0 as well as by the boundary-layer thickness δ_θ. The grids are seen to be stretched, at rates lower than 4% to preserve numerical accuracy. This enables to avoid an excessive number of grid points, and to discretize the inlet boundary layer by 19 points using 62 points within the pipe radius. The maximum radial mesh spacing is obtained outside the jet flow for $r \geq 3r_0$, and is equal to $\Delta r = 0.065r_0$. The time frequency f of acoustic waves discretized by four grid points in this case corresponds to Strouhal number $\mathrm{St} = fD/u_j = 8.6$. The radial mesh spacings in Jetv9ring256drdz are also shown in figure 1 overall to vary similarly to the spacings in the other simulations. The resolution around $r = r_0$ is however twice as fine, and there are now 31 grid points in the boundary layer for 77 points within the pipe radius. Finally, regarding the quality of discretization of the shear layers, it can be noted that Δr is for instance lower than $\delta_\theta/2$ over $0.85r_0 \leq z \leq 1.15r_0$ in all LES.

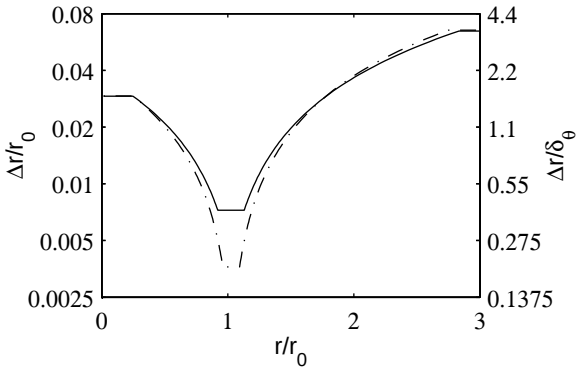

Figure 1. Representation, in logarithmic scales, of the mesh spacing Δr in the radial direction, normalized by r_0 (left y-axis) or by δ_θ (right y-axis), in: ——— Jetv9noise256, Jetv9ring256, Jetv9ring512, and Jetv9ring1024dz, — · — · Jetv9ring256drdz,

The variations in grid resolution along the lip line in the different simulations are displayed in figure 2. As expected, the radial and azimuthal mesh spacings are constant, and remain equal to their values at the nozzle lip given in table 2. Concerning the discretization in the azimuthal direction, it can in particular be remarked that $r_0\Delta\theta = 1.36\delta_\theta$ in the three LES using $n_\theta = 256$, which is rather coarse, whereas $r_0\Delta\theta = 0.68\delta_\theta$ using $n_\theta = 512$ and $r_0\Delta\theta = 0.34\delta_\theta$ using $n_\theta = 1024$.

As for the discretization in the axial direction, the mesh spacings are minimum around the pipe exit, but they increase upwards and downwards to save grid points. They remain however uniform in the pipe over $-r_0 \leq z \leq 0$, that is between the trip location and the nozzle exit. Upstream of $z = -r_0$, the grids are stretched up to the inlet, so that there are 98 points in the pipe in Jetv9noise256, Jetv9ring256 and Jetv9ring512, and 169 points in Jetv9ring256drdz and Jetv9ring1024dz. Downstream of the nozzle, a grid stretching is also applied at rates lower than 1%, to reach $\Delta z = 0.065r_0$ at $z = 5.7r_0$ in Jetv9noise256, Jetv9ring256 and Jetv9ring512, at $z = 7.8r_0$ in Jetv9ring256drdz, and at $z = 13.3r_0$ in Jetv9ring1024dz. The axial grid resolution is therefore significantly higher in the final simulation, around the nozzle lip but also farther downstream nearly up to the end of the jet potential core. To illustrate this, compare for instance the mesh spacings at $z = 1.5r_0$ and at $z = 6r_0$: they are respectively $\Delta z = 1.5\delta_\theta$ and $\Delta z = 3.6\delta_\theta$ in Jetv9ring512, but $\Delta z = 0.7\delta_\theta$ and $\Delta z = 1.8\delta_\theta$ in Jetv9ring1024dz.

The numbers of time steps and the non-dimensional simulation times Tu_j/D of the different simulations are provided in table 2. From 81,000 up to 110,000 iterations have been done, corresponding to physical times between $325r_0/u_j$ to $475r_0/u_j$. To study jet turbulence features and to perform far-field acoustic extrapolation, density, velocity components and pressure are recorded from time $t = 125r_0/u_j$ at every point along the centerline at $r = 0$, and on cylindrical surfaces located at $r = r_0$ and at $r = 7.25r_0$, at a frequency

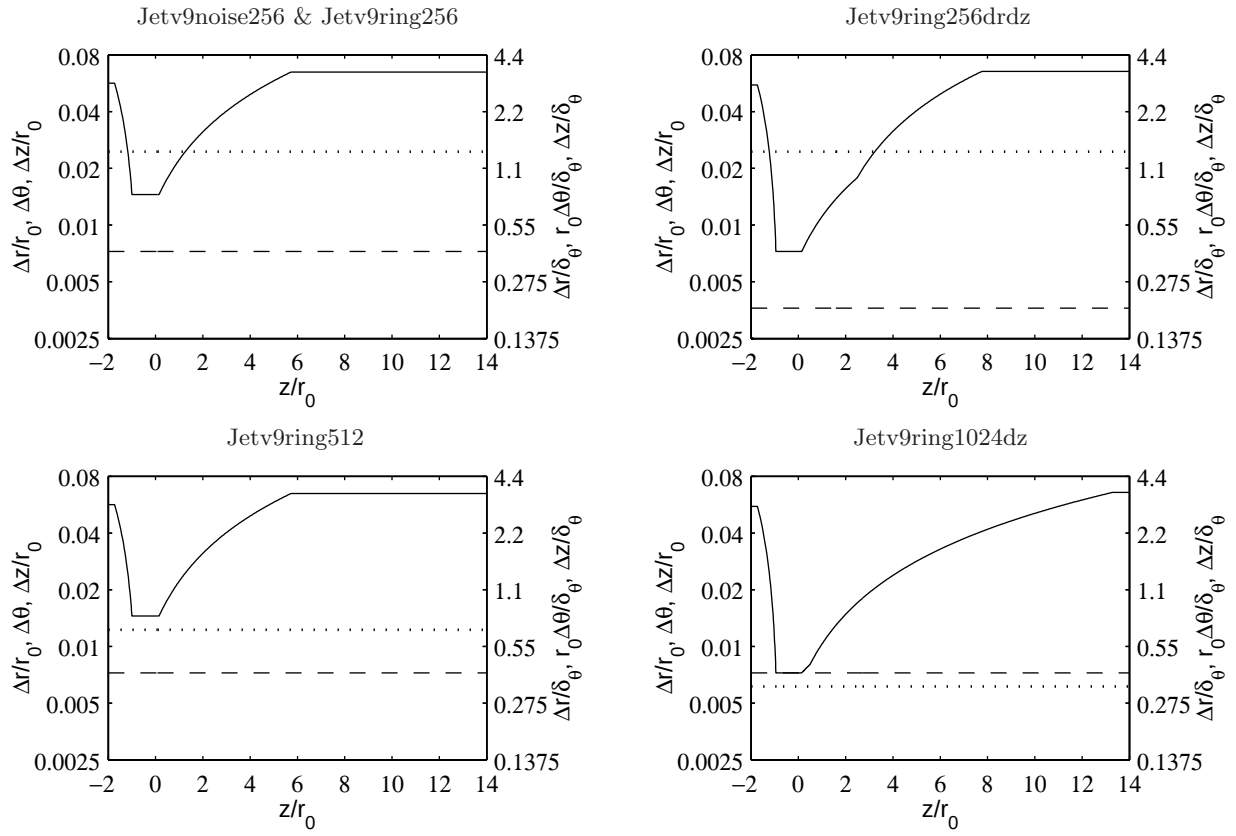

Figure 2. Representation, in logarithmic scales, of the mesh spacings in the axial, radial and azimuthal directions at $r = r_0$, in the different simulations: ——— Δz, − − − Δr, ····· $r_0\Delta\theta$. They are normalized by the jet radius r_0 (left y-axis) or by the exit boundery-layer momentum thickness δ_θ (right y-axis).

allowing the computation of spectra up to Strouhal number 20. The velocity spectra are moreover evaluated from overlapping samples of duration $27.4r_0/u_j$. The flow statistics are also determined from $t = 175r_0/u_j$, and results are averaged in the azimuthal direction.

The LES have been carried out using NEC SX-8 computers. The simulation Jetv9ring1024dz has particularly been performed on 7 processors using OpenMP, at a CPU speed around 36 Gflops, and required around 4000 CPU hours and 60 Go of memory.

C. Nozzle-exit conditions

In this section, the flow conditions obtained at the nozzle exit of the jets are examined. The mean and rms turbulent profiles calculated for the axial velocity at $z = 0$ are first shown in figure 3. In all jets, the profiles of mean velocity $< u_z >$ do not differ appreciably from the Blasius boundary-layer profile of momentum thickness $\delta_\theta = 0.018r_0$ imposed at the pipe inlet. In the same way, the peak levels of velocity fluctuations are all around 9% of the jet velocity, even if the rms profiles are found to vary with the tripping method. Tripping the boundary layers with random vortical disturbances indeed appears to generate large turbulent intensities on a slightly wider radial region. Notwithstanding, the present jets all exhibit the same nozzle-exit conditions, in agreement with those measured in the initially nominally turbulent, highly disturbed jets considered in Zaman's experiments.[7,10] It can also be noted that the Reynolds number based on the exit boundary-layer momentum thickness is $\mathrm{Re}_\theta = 900$.

As pointed out by Bridges and Hussain[11] for instance, mean and rms velocity profiles may not be sufficient to characterize jet initial conditions, and velocity spectra should additionally be provided. Accordingly, spectra of axial velocity u'_z are computed in the jets just downstream of the nozzle lip at $r = r_0$ and $z = 0.4r_0$. They are represented in figure 4 as functions of Strouhal number $\mathrm{St} = fD/u_j$ but also of azimuthal wave number k_θ, to identify both frequential and azimuthal components of the early shear-layer velocity disturbances. It can first be noticed that the velocity spectra from Jetv9noise256 and Jetv9ring256

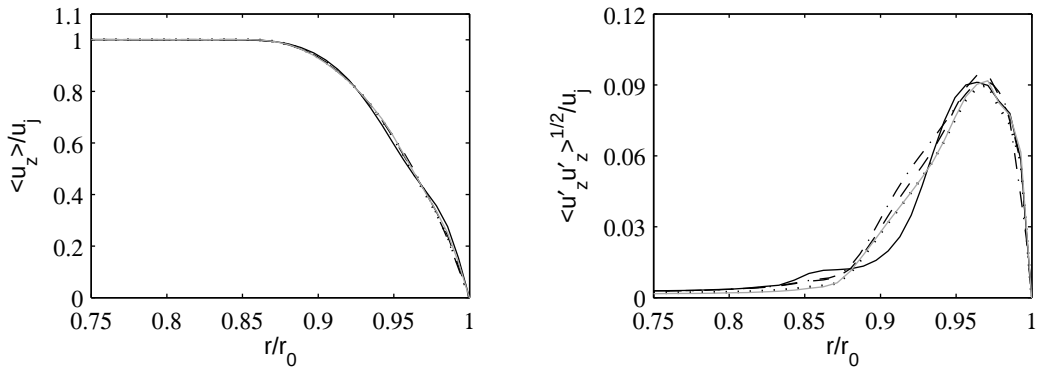

Figure 3. Profiles at $z = 0$ of mean axial velocity $< u_z >$, and of the rms values of fluctuating axial velocity u'_z, for: ——— Jetv9noise256, − − − Jetv9ring256, − · − · Jetv9ring256drdz, ····· Jetv9ring512, ——— Jetv9ring1024dz.

are remarkably similar, which suggests that the physical features of the jet initial turbulence do not depend much on the tripping method. In all cases, the frequency spectra also do not contain any distinct peak that might appear using an unappropriate trip device or a numerical set-up generating forced turbulence. Instead, the spectra are all broadband, and even rather flat for St ≤ 1 as it could be obtained for white noise. This indicates that the jet initial conditions are satisfactorily clean.

Concerning the azimuthal velocity spectra, they are all broadband, revealing significant components up to high wave numbers k_θ, which supports that no mode strongly dominates at the jet exit. In Jetv9noise256, Jetv9ring256 and Jetv9ring256drdz in particular, using $n_\theta = 256$, the spectra are flat for $k_\theta \leq 16$, then reach maximum values for $k_\theta \simeq 32$, and finally sharply collapse around $k_\theta = 64$ as typically observed for a spectral truncation. The latter wave number corresponds to the cut-off wave number of the relaxation filtering that is obtained approximately for four points per wavelength. In Jetv9ring512 and Jetv9ring1024dz, using respectively $n_\theta = 512$ and $n_\theta = 1024$, the azimuthal spectra, while being in overall agreement with previous spectra, are however smoother. The components of larger amplitude, which are now found at $k_\theta \simeq 38$, are less pronounced, and there is no abrupt decrease of the spectra at high wave numbers. The turbulent energy is also distributed on higher modes between $k_\theta = 64$ and $k_\theta = 128$.

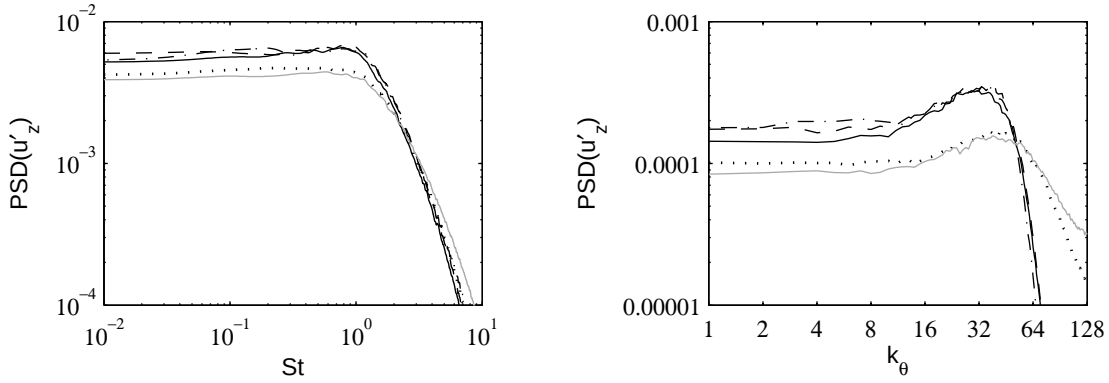

Figure 4. Power spectral densities of axial fluctuating velocity u'_z as functions of Strouhal number St $= fD/u_j$ (left), and of azimuthal wave number k_θ (right), at $z = 0.4r_0$ and $r = r_0$ for: ——— Jetv9noise256, − − − Jetv9ring256, − · − · Jetv9ring256drdz, ····· Jetv9ring512, ——— Jetv9ring1024dz.

D. Far-field extrapolation

The near fields obtained by LES are propagated to the far field using the wave-extrapolation methodology developed in recent simulations,[34,46] by solving the linear acoustic equations written in cylindrical coordinates for the fluctuating velocity components and pressure. The numerical schemes and boundary conditions used are the same as those implemented in the LES. Non-centered finite differences and filters are in particular applied at the inner-side boundary of the extrapolation grid.

In practice, the far-field extrapolation is performed from velocities and pressure recorded in the LES from time $t = 125r_0/u_j$ at every point at $r = 7.25r_0$, at a frequency allowing the computation of spectra up to Strouhal number 20. These data are interpolated on a cylindrical surface discretized by a uniform mesh spacing $\Delta z = 0.065r_0$ in the axial direction. They are then imposed at the bottom boundary of a cylindrical grid of $n_r \times n_\theta \times n_z = 835 \times 256 \times 1155$ points, extending axially from $z = -16.6r_0$ to $z = 58.2r_0$ and radially up to $r = 61.4r_0$, on which the linear acoustic equations are solved. The mesh spacings of the grid are uniform with $\Delta r = \Delta z = 0.065r_0$, yielding Strouhal number St = 8.6 for the sound waves discretized by four grid points. After a propagation time of $t = 60r_0/u_j$, pressure is recorded around the jets at points located at $60r_0$ from $z = r = 0$, during time periods of $300r_0/u_j$ for Jetv9noise256, Jetv9ring256 and Jetv9-ring512, $140r_0/u_j$ for Jetv9ring256drdz, and $290r_0/u_j$ for Jetv9ring1024dz. Pressure spectra are evaluated using overlapping samples of duration $38r_0/u_j$, and they are also averaged in the azimuthal direction.

III. Aerodynamic fields

A. Shear-layer development

To illustrate the shear-layer development just downstream of the nozzle lip in the five computed jets, snapshots of the vorticity norm obtained over $0 \leq z \leq 3r_0$ are first presented in figure 5. As expected in initially nominally turbulent jets, vortical structures are found immediately from the exit section at $z = 0$. Both small and large structures are also observed in agreement with the Reynolds number $\mathrm{Re}_D = 10^5$. A wider range of fine turbulent scales can however be noticed in the simulations using finer grids, especially in Jetv9ring1024dz, whereas coherent structures may be more apparent in Jetv9noise256 and Jetv9ring256 using coarser grids.

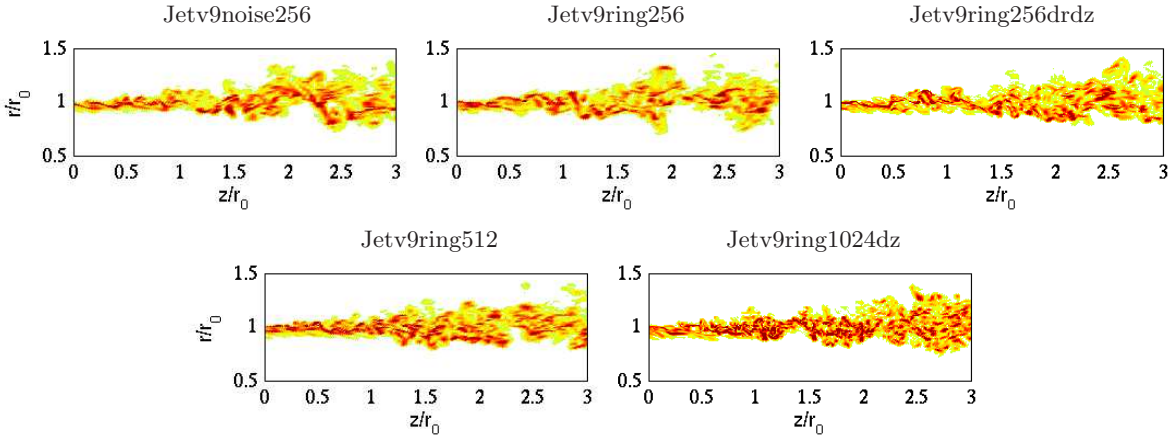

Figure 5. Snapshots in the (z, r) plane of vorticity norm $|\omega|$ just downstream of the pipe lip for the different jets. The color scale ranges up to the level of $25u_j/r_0$.

To quantify the size of the turbulent structures in the mixing layers, axial and azimuthal integral length scales $L_{uu}^{(z)}$ and $L_{uu}^{(\theta)}$ have been calculated from velocity u_z' at $r = r_0$. Their values at $z = 0.4r_0$, provided in table 3, are found to depend mainly on the azimuthal mesh resolution. Both $L_{uu}^{(z)}$ and $L_{uu}^{(\theta)}$ are for example reduced by roughly 25% when the number of points in the azimuth increases from $n_\theta = 256$ to $n_\theta = 1024$. It can also be worth noting that in all jets the initial azimuthal length scales are about four times smaller than the axial length scales, e.g. $L_{uu}^{(\theta)} = 0.013r_0$ versus $L_{uu}^{(z)} = 0.061r_0$ in Jetv9ring1024dz, which may be important when fixing the grid parameters.

The variations of the integral length scales along the lip line up to the position $z = 12r_0$, that is close to the end of the jet potential core as it will be shown later, are presented in figure 6. As typically found in experiments, from the works by Davies *et al.*[47] to the recent PIV measurements of Fleury *et al.*[48] also plotted in the figure, the length scales are observed to grow fairly linearly. They are not basically different, especially in the three jets Jetv9noise256, Jetv9ring256 and Jetv9ring256drdz. Downstream of $z = 4r_0$, the axial length scales $L_{uu}^{(z)}$ are however visibly larger in Jetv9ring1024dz than in other jets, thus leading to a better agreement with the experimental data obtained by Fleury *et al.*[48] for a jet at M = 0.9 and $\mathrm{Re}_D = 7.7 \times 10^5$. The azimuthal length scales $L_{uu}^{(\theta)}$ seem less scattered, even in they may persistantly be

Table 3. Axial and azimuthal integral length scales $L_{uu}^{(z)}$ and $L_{uu}^{(\theta)}$ calculated from velocity u_z' at $r = r_0$ and $z = 0.4r_0$, and peak rms values of axial and radial fluctuating velocities u_z' and u_r' along the shear layer.

simulation	$L_{uu}^{(z)}/r_0$	$L_{uu}^{(\theta)}/r_0$	$<u_z'^2>^{1/2}/u_j$	$<u_r'^2>^{1/2}/u_j$
Jetv9noise256	0.078	0.018	0.175	0.138
Jetv9ring256	0.078	0.019	0.175	0.136
Jetv9ring256drdz	0.076	0.022	0.177	0.135
Jetv9ring512	0.067	0.016	0.158	0.125
Jetv9ring1024dz	0.061	0.013	0.157	0.117

slightly smaller in the jets simulated using higher azimuthal resolution.

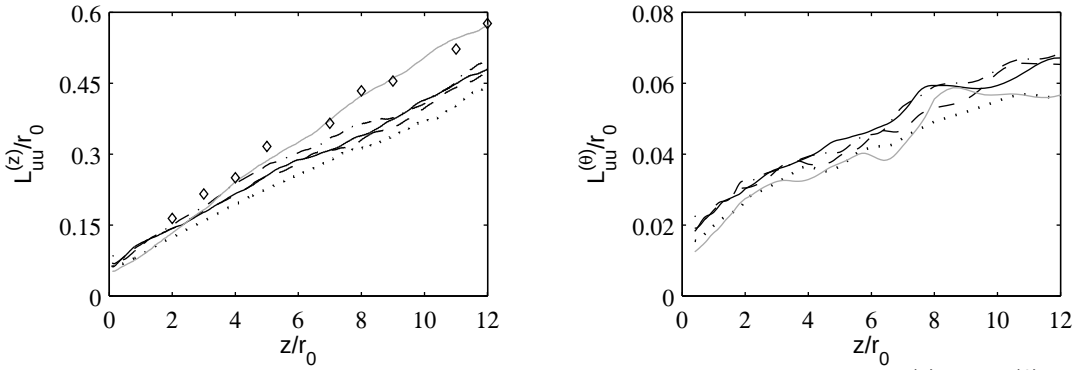

Figure 6. Variations along the lip line of the axial and azimuthal integral length scales $L_{uu}^{(z)}$ and $L_{uu}^{(\theta)}$ calculated from velocity u_z' at $r = r_0$ for: ——— Jetv9noise256, − − − Jetv9ring256, − · − · Jetv9ring256drdz, ····· Jetv9ring512, ——— Jetv9ring1024dz. Measurements: ◇ Fleury *et al.*[48] for a Mach 0.9 jet at $\mathrm{Re}_D = 7.7 \times 10^5$.

To discuss the quality of discretization of the turbulent structures developing in the jet mixing layers, ratios between the integral velocity length scales and the mesh spacings have been calculated at $r = r_0$. The variations of $L_{uu}^{(z)}/\Delta z$ and $L_{uu}^{(\theta)}/(r_0\Delta\theta)$ along the lip line are represented in figure 7 up to $z = 12r_0$. Their values at the specific positions of $z = 0.4r_0$, $z = 1.5r_0$, $z = 3r_0$ and $z = 6r_0$ are collected in table 4. The axial length scales $L_{uu}^{(z)}$ in Jetv9noise256, Jetv9ring256 and Jetv9ring512 first appear to be discretized by fewer than 5 points upstream of $z = 7r_0$, then by more points downstream because of the growth of turbulent scales in the axial direction. In Jetv9ring512 in particular, $L_{uu}^{(z)}$ strikingly remains equal to $4\Delta z$ up to $z = 6r_0$, as quantified in table 4. Therefore the axial grid resolution in the three jets mentioned above may be sufficient, but the accuracy might be low, especially considering the relaxation filtering cut-off that is for about 4 points per wavelength. Fortunately this should not be the case in the two other simulations using finer axial discretizations. In Jetv9ring256drdz one indeed obtains for instance $L_{uu}^{(z)} = 9.09\Delta z$ initially at $z = 0.4r_0$ and still $L_{uu}^{(z)} = 6.11\Delta z$ at $z = 6r_0$, while in Jetv9ring1024dz $L_{uu}^{(z)} \geq 7.8\Delta z$ all along the mixing layer, which is very satisfactory given the low-dispersion low-dissipation numerical schemes used.

The numbers of grid points in the azimuthal integral velocity length scales are also seen to vary significantly in the present jets. In the three simulations Jetv9noise256, Jetv9ring256 and Jetv9ring256drdz, $L_{uu}^{(\theta)}$ is for instance smaller than $r_0\Delta\theta$ at $z = 0.4r_0$, which can be related to the spectral-like truncation observed in the corresponding azimuthal velocity spectra in figure 4. The length scales are moreover not discretized (*i.e.* $L_{uu}^{(\theta)} < 2r_0\Delta\theta$) upstream of $z = 7.5r_0$. This clearly indicates that the azimuthal grid resolution is insufficient in the LES using $n_\theta = 256$. The integral scales $L_{uu}^{(\theta)}$ are however found to be much better taken into account in the two simulations using $n_\theta = 512$ and $n_\theta = 1024$. In Jetv9ring512, they contain more than two grid points downstream of $z = 1.7r_0$, yielding for example $L_{uu}^{(\theta)} = 3.4r_0\Delta\theta$ at $z = 6r_0$. In Jetv9ring1024dz, more importantly, the integral scales are discretized immediately from the nozzle exit, with $L_{uu}^{(\theta)} = 2.04r_0\Delta\theta$ at $z = 0.4r_0$, and they are well calculated (*i.e.* $L_{uu}^{(\theta)} > 4r_0\Delta\theta$) downstream of $z = 1.7r_0$.

The mesh grid in Jetv9ring1024dz, which was shown in figure 2 to display high resolutions in all cylindrical

coordinate directions, therefore appears from figure 7 and table 4 as the only grid likely to provide mixing-layer solutions reaching a high level of confidence. For example, in Jetv9ring256drdz and in Jetv9ring512, the mesh spacings respectively in the axial and in the azimuthal directions might not be small enough to compute properly the turbulent structures in the shear layer.

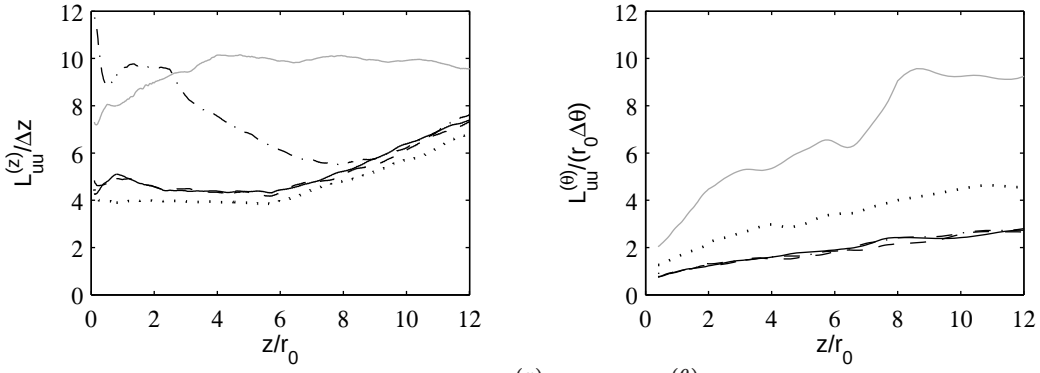

Figure 7. Variations along the lip line of the ratios $L_{uu}^{(z)}/\Delta z$ and $L_{uu}^{(\theta)}/(r_0\Delta\theta)$ between integral length scales calculated from velocity u_z', and mesh spacings, for: ——— Jetv9noise256, − − − Jetv9ring256, − · − · Jetv9ring256drdz, ····· Jetv9ring512, ——— Jetv9ring1024dz.

Table 4. Ratios $L_{uu}^{(z)}/\Delta z$ and $L_{uu}^{(\theta)}/(r_0\Delta\theta)$ between integral length scales calculated from velocity u_z' and mesh spacings for different positions at $r = r_0$. The values obtained for Jetv9noise256 are not reported because they are very similar to those for Jetv9ring256.

simulation	ratio	$z = 0.4r_0$	$z = 1.5r_0$	$z = 3r_0$	$z = 6r_0$
Jetv9ring256	$L_{uu}^{(z)}/\Delta z$	4.66	4.84	4.49	4.32
Jetv9ring256drdz	$L_{uu}^{(z)}/\Delta z$	9.09	9.66	8.41	6.11
Jetv9ring512	$L_{uu}^{(z)}/\Delta z$	4	4.04	3.96	3.95
Jetv9ring1024dz	$L_{uu}^{(z)}/\Delta z$	7.84	8.67	9.44	9.91
Jetv9ring256	$L_{uu}^{(\theta)}/(r_0\Delta\theta)$	0.78	1.12	1.45	1.83
Jetv9ring256drdz	$L_{uu}^{(\theta)}/(r_0\Delta\theta)$	0.92	1.12	1.45	1.82
Jetv9ring512	$L_{uu}^{(\theta)}/(r_0\Delta\theta)$	1.27	1.86	2.60	3.40
Jetv9ring1024dz	$L_{uu}^{(\theta)}/(r_0\Delta\theta)$	2.04	3.68	5.29	6.49

Coming back to the simulation output, the variations over $0 \leq z \leq 12r_0$ of the jet shear-layer momentum thickness are presented in figure 8. They are very similar in Jetv9noise256, Jetv9ring256 and Jetv9ring256drdz using $n_\theta = 256$ points in the azimuthal direction. Therefore the mean development of the mixing layers appears quite independent of the tripping methodology or of the axial and radial discretizations around the nozzle lip. The results from Jetv9ring512 and Jetv9ring1024dz however differ appreciably. As the azimuthal resolution becomes higher, the shear layer indeed spreads more slowly.

For comparison, measurements obtained by Husain and Hussain[9] for an initially turbulent axisymmetric mixing layer at a Mach number of 0.09 and a Reynolds number of 2.5×10^5, and by Fleury *et al.*[48] for a round jet at M = 0.9 and $\mathrm{Re}_D = 7.7 \times 10^5$ are also plotted in figure 8. While keeping in mind that comparisons between experimental and numerical data might be meaningless if the inflow conditions strongly disagree, they seem to better correspond to the profile determined in Jetv9ring1024dz, especially in the early stage of shear-layer growth.

The turbulent developments of the mixing layers are now characterized by showing in figure 9 the variations over $0 \leq z \leq 12r_0$ of the maximum values of rms velocities $<u_z'^2>^{1/2}$, $<u_r'^2>^{1/2}$ and $<u_\theta'^2>^{1/2}$, and of Reynolds shear stresses $<u_r'u_z'>$. Similar trends are noted for the different velocity components. The profiles of turbulent intensities from Jetv9noise256 and Jetv9ring256 are first seen to collapse very well, indicating that the influence of the tripping procedure is negligible. They are also close to the profiles from the simulation Jetv9ring256drdz using higher resolutions in the axial and radial directions while keeping $n_\theta = 256$ points in the azimuth. In these jets, the turbulent intensities reach remarkable peaks around $z = 2r_0$, of magnitudes $<u_z'^2>^{1/2} \simeq 0.175u_j$ and $<u_r'^2>^{1/2} \simeq 0.136u_j$ for instance as reported in table 3, which may

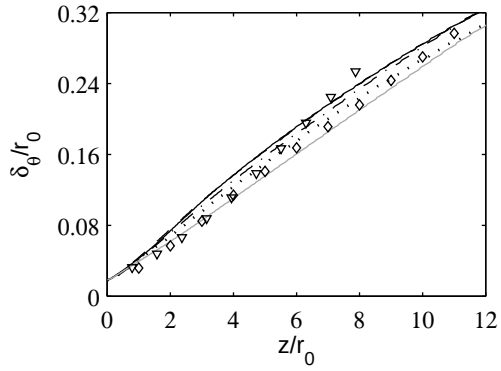

Figure 8. Variations of shear-layer momentum thickness δ_θ for: ——— Jetv9noise256, − − − Jetv9ring256, − · − · Jetv9ring256drdz, ····· Jetv9ring512, ——— Jetv9ring1024dz. Measurements: ▽ Husain and Hussain[13] for an initially turbulent axisymmetric shear layer, ◇ Fleury *et al.*[48] for a Mach 0.9 jet at $Re_D = 7.7 \times 10^5$.

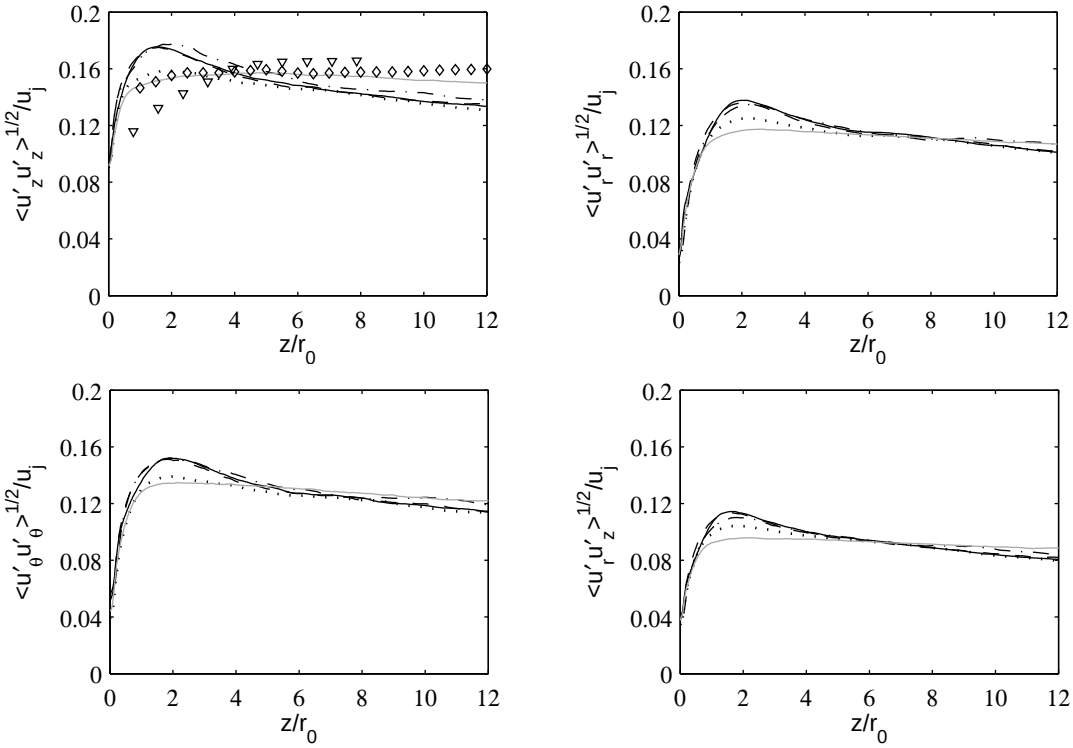

Figure 9. Variations of the peak rms values of fluctuating velocities u'_z, u'_r and u'_θ, and of the peak magnitudes of Reynolds shear stress $< u'_r u'_z >$ for: ——— Jetv9noise256, − − − Jetv9ring256, − · − · Jetv9ring256drdz, ····· Jetv9ring512, ——— Jetv9ring1024dz. Measurements: ▽ Husain and Hussain[13] for an initially turbulent axisymmetric shear layer, ◇ Fleury *et al.*[48] for a Mach 0.9 jet at $Re_D = 7.7 \times 10^5$.

be associated with strong shear-layer transitions. As more points are specified in the azimuthal direction, the rms velocity profiles are modified in an important manner. The profiles obtained from Jetv9ring512 and Jetv9ring1024dz using $n_\theta = 512$ and $n_\theta = 1024$ points thus exhibit initially smoother shapes and lower peak values, equal respectively to $0.158u_j$ and $0.157u_j$ for u'_z, and to $0.125u_j$ and $0.117u_j$ for u'_r. Downstream of $z \simeq 5r_0$, the turbulent intensities from Jetv9ring512 and Jetv9ring1024dz however vary in different ways. In the former case, they decrease as in the first three simulations, whereas in the latter case they remain high, leading to rms axial velocity profiles increasing nearly monotonically.

Such behaviours can be connected to the resolution properties presented in figure 7. It was indeed shown that using $n_\theta = 256$ points the turbulent structures are very poorly taken into account downstream of the exit section, which may strengthen the mixing-layer transition in Jetv9noise256, Jetv9ring256, and Jetv9ring256drdz. The axial discretization in Jetv9ring512, which is the same as that in Jetv9noise256 and Jetv9ring256, was also found to be insufficient along the shear layer, which may result in the low turbulence levels noticed for $z \geq 6r_0$. On the contrary, Jetv9ring1024dz can be expected to provide trustworthy solutions both for the early and for the downstream developments of the jet mixing layer.

As done previously in figure 8, experimental data from Husain and Hussain[9] and from Fleury *et al.*[48] are depicted in figure 9, for the rms axial velocities. Despite significant discrepancies, likely originating from discrepancies in the initial conditions, their overall variations better agree with the turbulent intensity profile from Jetv9ring1024dz. This is specially the case for the measurements from Fleury *et al.*[48]

B. Jet flow development

To visualize the turbulent jet development, snapshots of the vorticity fields obtained in the five simulations up to $z = 25r_0$ are represented in figure 10. No appreciable difference in the jet flow fields can be clearly distinguished. In all cases for instance, the end of the jet potential core appears to be located around 15 radii downstream of the nozzle exit.

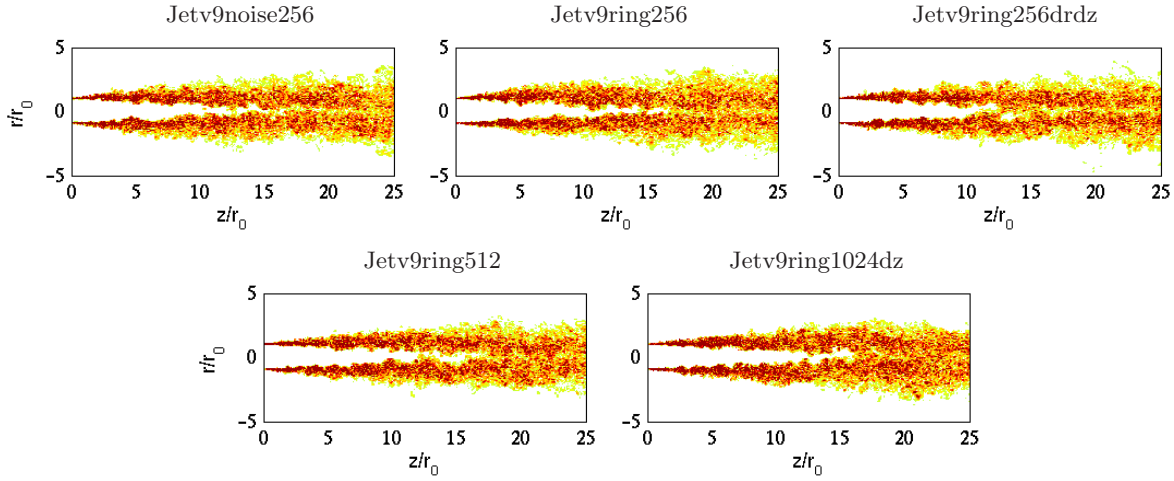

Figure 10. Snapshots in the (z, r) plane of vorticity norm $|\omega|$ for the jet flow fields up to $z = 25r_0$. The color scale ranges up to the level of $5u_j/r_0$.

The variations of the centerline mean axial velocity u_c and of the half-width $\delta_{0.5}$ of the jets are presented in figure 11. In the same way as for the mixing layers in figure 8, the mean developments of the jets are almost identical in the three simulations using $n_\theta = 256$ points in the azimuth, despite various tripping methods and axial and radial discretizations at the nozzle lip. Jetv9noise256, Jetv9ring256 and Jetv9ring256drdz thus all display potential cores of lengths $z_c \simeq 15.5r_0$, where z_c is arbitrarily defined by $< u_z > (z = z_c) = 0.95u_j$, as reported in table 5. The jet mean flows however develop differently in Jetv9ring512 and in Jetv9ring1024dz. They spread indeed farther downstream in the former case, but inversely slightly earlier and more rapidly in the latter case, yielding potential cores of respective lengths $z_c = 16.4r_0$ and $z_c = 15.2r_0$.

Measurements obtained for jets at Mach number 0.9 by Lau *et al.*,[49] Arakeri *et al.*,[17] and Fleury *et al.*[48] are also represented in figure 11. They better agree with the mean flow profiles provided by Jetv9ring1024dz. Note that the comparisons with the present simulation results can reasonably be regarded as meaningful, because the experimental jets are at Reynolds numbers higher than 5×10^5. Therefore, albeit possibly

initially laminar, they probably all contain significant inflow turbulence. This is the case for instance in the jet of Arakari *et al.*,[17] in which the peak rms values of u'_z at the exit section are around 10% u_j.

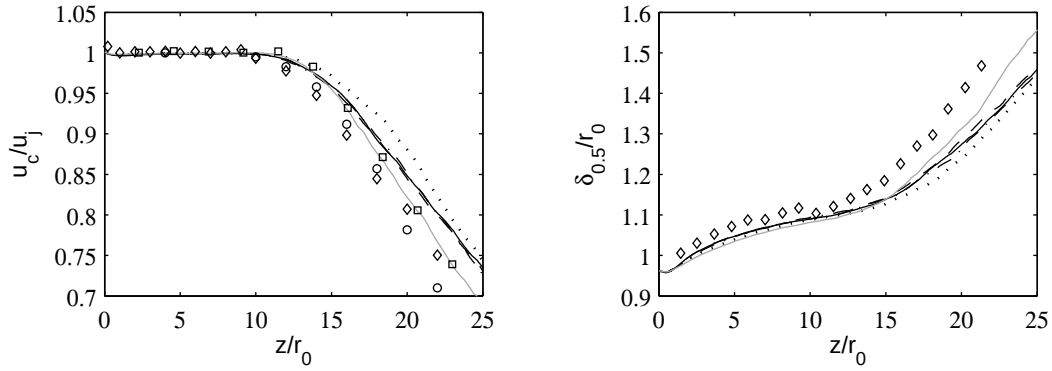

Figure 11. Variations of centerline mean axial velocity u_c and of jet half-width $\delta_{0.5}$ for: ——— Jetv9noise256, − − − Jetv9ring256, − · − · Jetv9ring256drdz, ····· Jetv9ring512, ——— Jetv9ring1024dz. Measurements for Mach 0.9 jets at $Re_D \geq 5 \times 10^5$: ○ Lau *et al.*,[49] □ Arakeri *et al.*,[17] ◇ Fleury *et al.*[48]

Table 5. Axial position of the end of the potential core z_c, and peak rms values of axial and radial fluctuating velocities u'_z and u'_r at $r = 0$ and $z = z_c$.

simulation	z_c/r_0	$<u_z'^2>^{1/2}/u_j$	$<u_r'^2>^{1/2}/u_j$
Jetv9noise256	15.6	0.071	0.053
Jetv9ring256	15.4	0.072	0.056
Jetv9ring256drdz	15.6	0.070	0.046
Jetv9ring512	16.4	0.067	0.049
Jetv9ring1024dz	15.2	0.082	0.069

The developments of the jets are finally illustrated by the centerline rms values of fluctuating velocities u'_z and u'_r plotted in figure 12, and compared as previously with experimental data from Lau *et al.*,[49] Arakeri *et al.*,[17] and Fleury *et al.*[48] As it could be expected from the preceding results indicating very weak influence of the tripping methodology, the profiles from Jetv9noise256 and Jetv9ring256 are first seen to collapse. The turbulent intensities are then found to be lower in Jetv9ring256drdz and Jetv9ring512, but significantly higher in Jetv9ring1024dz. At the end of the potential core, at $r = 0$ and $z = z_c$, the rms axial velocities thus range for instance from $0.067u_j$ in Jetv9ring512 to $0.082u_j$ in Jetv9ring1024dz, and the rms radial velocities are from $0.046u_j$ in Jetv9ring256drdz to $0.069u_j$ in Jetv9ring1024dz, see the values collected in table 5 for all jets. In this way also, the centerline turbulent intensities in Jetv9ring1024dz satisfactorily correspond to the measurements, whereas they are of lesser magnitude in the four other cases.

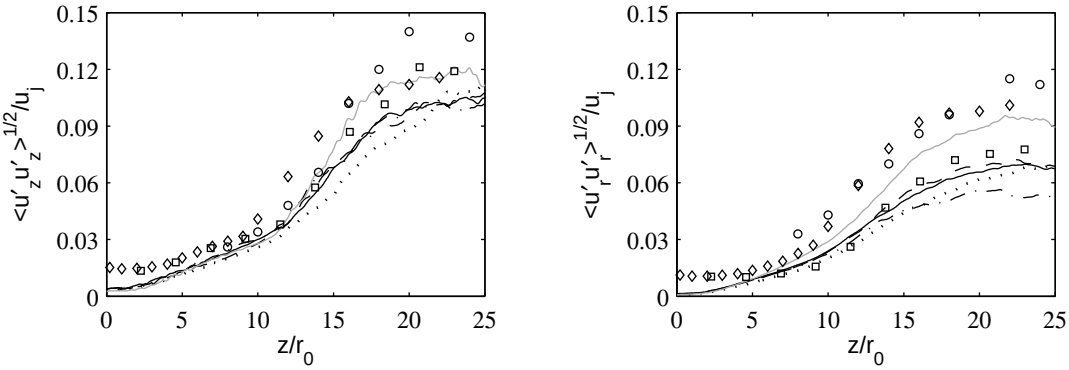

Figure 12. Variations along jet centerline at $r = 0$ of the rms values of fluctuating velocities u'_z and u'_r for: ——— Jetv9noise256, − − − Jetv9ring256, − · − · Jetv9ring256drdz, ····· Jetv9ring512, ——— Jetv9ring1024dz. Measurements for Mach 0.9 jets at $Re_D \geq 5 \times 10^5$: ○ Lau *et al.*,[49] □ Arakeri *et al.*,[17] ◇ Fleury *et al.*[48]

IV. Acoustic fields

A. Near pressure fields

To give first insights into the noise radiated by the jets, snapshots of fluctuating pressure obtained directly by LES in the near field are presented in figure 13. Even if isolated snapshots might be misleading, and must consequently be interpreted with great caution, the pressure fields appear rather clean. Sound waves are also visibly coming from the flow region located around $z = 2r_0$, where the shear-layer transition takes place as shown in section II.A. They may however be of lower amplitude in the two bottom jets than in three top jets computed using coarser azimuthal mesh grids. To capture this, compare for instance the pressure fields from Jetv9noise256 (top left) and from Jetv9ring1024dz (bottom right).

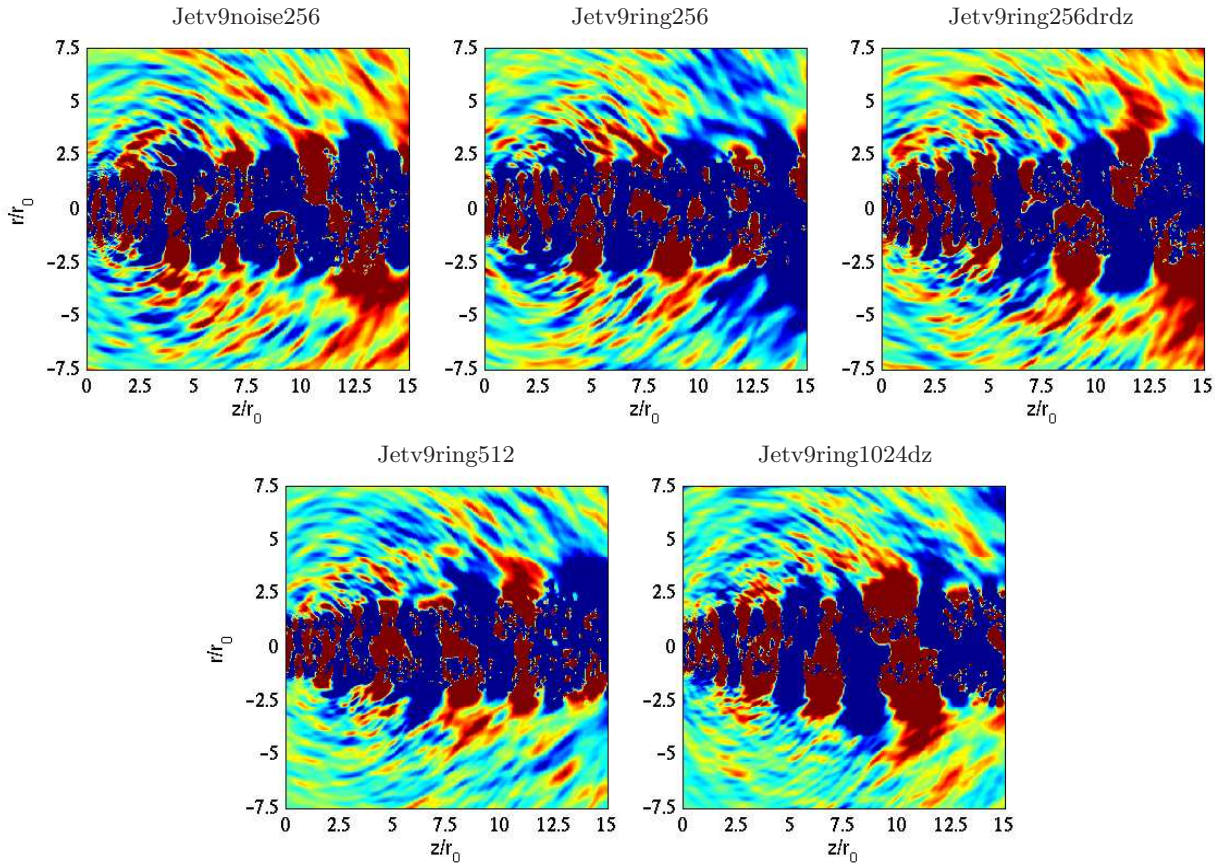

Figure 13. Snapshots in the (z, r) plane of fluctuating pressure $p - p_{amb}$ obtained by LES for the different jets. The color scale ranges for levels from -100 Pa to 100 Pa.

B. Far pressure fields

The LES near fields have been propagated to a distance of 60 radii from the nozzle exit, where far-field acoustic conditions are expected to apply according to experimental results.[50] The wave extrapolation is performed by solving the linear acoustical equations, using the same methodology as in previous simulations,[34] from a cylindrical control surface located at $r = 7.25r_0$ as described in section II.D. Two illustrations are given in figure 14 with pressure snapshots obtained for Jetv9ring256 and for Jetv9ring1024dz. The propagation of the sound waves generated by the turbulent jets seems properly calculated, even if there might unfortunately be some spurious low-frequency waves originating from the downstream part of the control surface as discussed in a recent paper.[34] Concerning the noise radiated by the two jets considered in the figure, it may appear somewhat lower in Jetv9ring1024dz than in Jetv9ring256, especially in the sideline direction, which will be quantified hereafter by sound pressure directivities and spectra.

The overall sound pressure levels calculated at $60r_0$ from the jet nozzle exit are presented in figure 15 for angles ϕ relative to the flow direction between 30° and 100°. The noise directivities from Jetv9noise256,

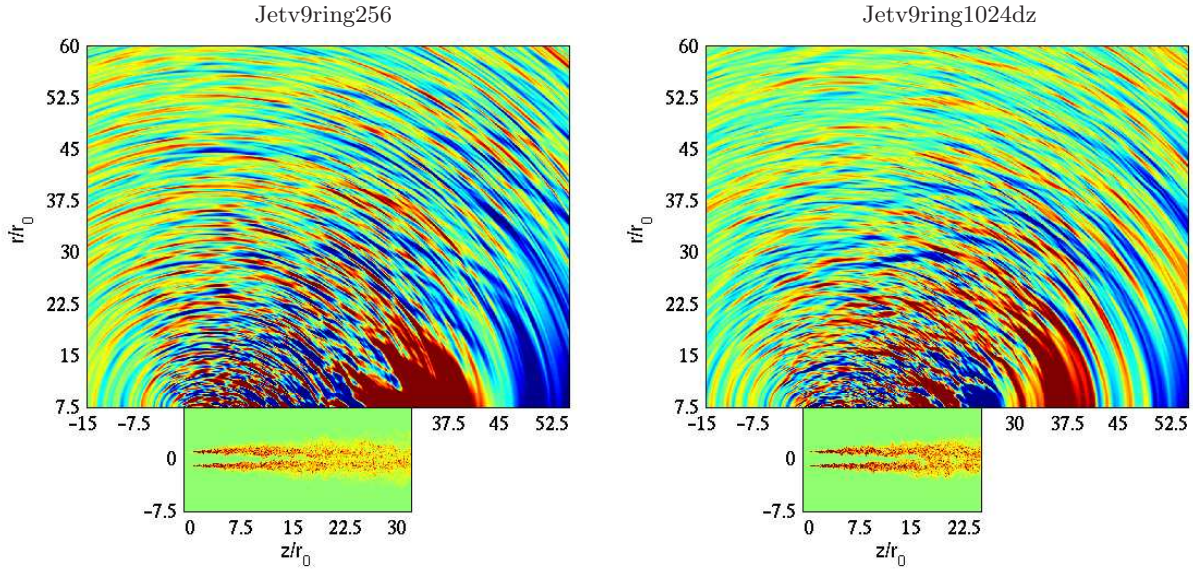

Figure 14. Snapshots in the (z, r) plane of the pressure field obtained from the acoustical simulations for Jetv9ring256 and Jetv9ring1024dz. The color scale ranges for levels from -16 Pa to 16 Pa.

Jetv9ring256 and Jetv9ring256drdz are nearly superimposed, which is not surprising given the very similar mean and turbulent developments of these jets evidenced in section III. In the same way, those from simulations Jetv9ring512 and Jetv9ring1024dz using higher azimuthal resolutions do not differ much except for $\phi < 50^o$, and both show constantly lower levels with respect to the first three cases. All over the range of radiation angles $50^o \leq \phi \leq 100^o$, noise reduction is about 1.5 dB. At the angle $\phi = 30^o$, it is also close to 1.5 dB in Jetv9ring1024dz, but it reaches 4 dB in Jetv9ring512.

Compared to the measurements obtained by Mollo-Christensen *et al.*,[51] Lush[52] and Bogey *et al.*[54] for Mach number 0.9 jets at $\mathrm{Re}_D \geq 5 \times 10^5$, also plotted in figure 15, the sound pressure levels determined for the present tripped jets at $\mathrm{Re}_D = 10^5$ are larger for most emission angles. For $\phi \geq 50^o$, they are more precisely higher by 4 dB in Jetv9noise256, Jetv9ring256 and Jetv9ring256drdz, and by 2.5 dB in Jetv9ring512 and Jetv9ring1024dz. For $\phi \simeq 30^o$, numerical and experimental data however correspond fairly well, apart from Jetv9ring512 resulting in significantly lower acoustic levels.

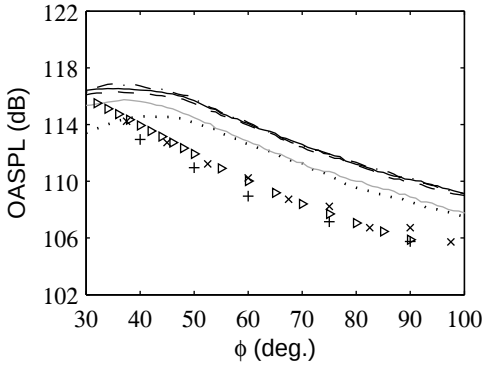

Figure 15. Sound pressure levels obtained at $60r_0$ from the pipe exit, as functions of the radiation angle relative to the jet direction, for: ——— Jetv9noise256, − − − Jetv9ring256, − · − · Jetv9ring256drdz, ·· ····· Jetv9ring512, ——— Jetv9ring1024dz. Measurements for jets at $\mathrm{Re}_D \geq 5 \times 10^5$: + Mollo-Christensen *et al.*,[51] × Lush,[52] ▷ Bogey *et al.*[54]

To provide further information on jet noise components, the far-field sound spectra estimated at the radiation angles $\phi = 30^o$, 40^o, 60^o and 90^o are represented in figure 16. The spectra from Jetv9noise256, Jetv9ring256 and Jetv9ring256drdz are almost the same, as expected from previous results. For Strouhal numbers lower than 0.5, they agree rather well with measurements for jets at Reynolds numbers higher than 7.8×10^5, whereas additional humps are observed for higher Strouhal numbers. These humps are broadband,

and their peaks are located around the frequency determined from the initial shear-layer momentum thickness using $f\delta_\theta/u_j = 0.0065$. This frequency is half of the frequency $f\delta_\theta/u_j = 0.013$ lying in the range of most-amplified frequencies initially measured in axisymmetric mixing layers.[3] The additional humps in the sound spectra can therefore be attributed to the first stage of vortex pairings in the shear layer, as found for instance in initially laminar jets.[7,11,34] They can in addition be connected to the strong mixing-layer transitions displayed in figure 9 in the three jets simulated using $n_\theta = 256$ points.

The latter contention is supported by the fact that, as the shear-layer transitions are smoother in Jetv9 ring512 and Jetv9ring1024dz as shown in figure 9, the additional humps in the corresponding sound spectra are attenuated approximately by 2 dB in figure 16. The acoustic fields of these two jets computed with higher grid resolutions thus still contain noticeable vortex-pairing noise. The presence of vortex pairings in the jet considered in the present study may result from a combination of physical reasons. They will be investigated in future works, but some hypotheses are listed below. First, the jet, albeit tripped so as to exhibit peak turbulent intensities of 9% at the nozzle exit, is initially transitional but not fully turbulent.[7] Second, the flow Reynolds numbers $\mathrm{Re}_D = 10^5$ and $\mathrm{Re}_\theta = 900$ are moderate. The diameter-based Reynolds number is in particular not higher than the barrier value of $\mathrm{Re}_D = 10^5$ which distinguishes low and high Reynolds number jet features according to some authors.[5,6] Finally the issue of the perseverance of coherent structures in turbulent mixing layers can be mentioned.[19]

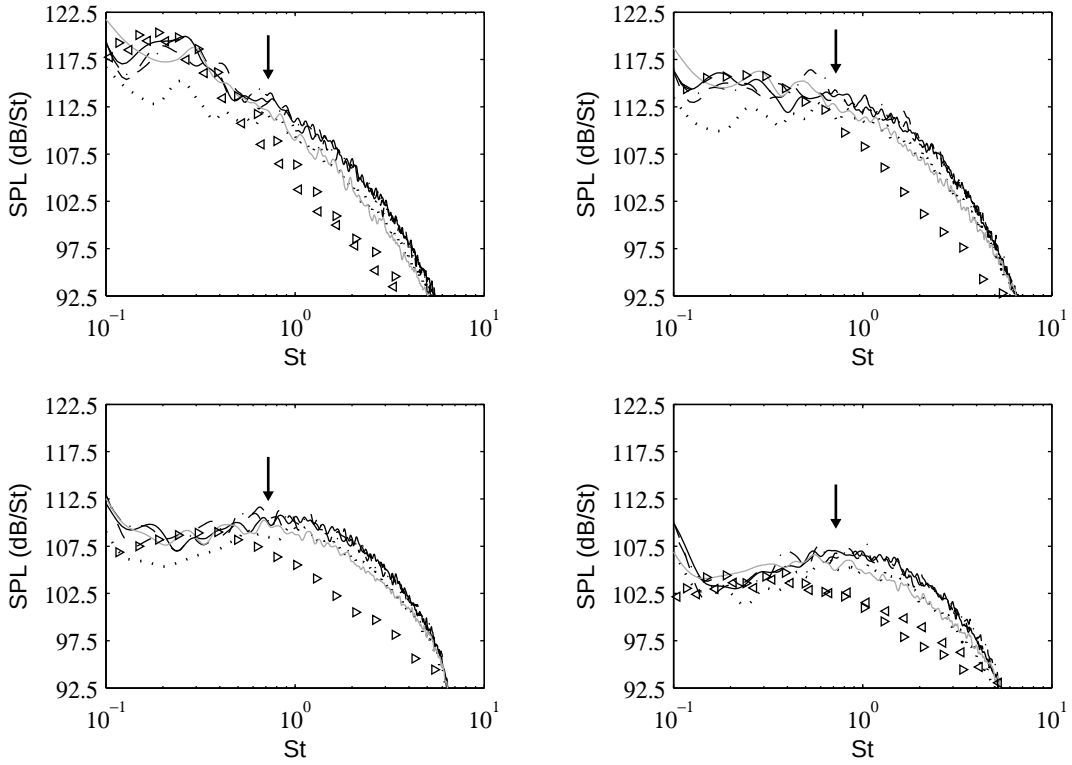

Figure 16. Sound pressure spectra obtained at $60r_0$ from the jet exit, as functions of Strouhal number $\mathrm{St} = fD/u_j$, for radiation angles of: 30^o (top left), 40^o (top right), 60^o (bottom left), and 90^o (bottom right), for: ——— Jetv9noise256, − − − Jetv9ring256, − · − · Jetv9ring256drdz, ····· Jetv9ring512, ——— Jetv9ring1024dz. The arrows indicate the frequency determined from the initial shear-layer thickness using $f\delta_\theta/u_j = 0.0065$. Measurements for jets at $\mathrm{Re}_D \geq 7.8 \times 10^5$: ◁ Tanna,[53] ▷ Bogey *et al.*[54]

It is interesting to note that the sound spectra from Jetv9ring512, and those from Jetv9ring1024dz using twice-as-fine axial and azimuthal discretizations do not appreciably differ for Strouhal numbers higher than 0.6. Consequently it is unlikely that the high-frequency components in the spectra, including vortex-pairing noise, be significantly affected by a further increase of the grid resolution. On the contrary, the sound spectra from Jetv9ring512 and from Jetv9ring1024dz show discrepancies for $\mathrm{St} \leq 0.6$. In Jetv9ring512, the low-frequency noise components appear underestimated with respect to the experimental data for all emission angles. This point can be related to the coarse axial discretization in this simulation leading to low turbulent intensities on the centerline around the end of the potential core, refer to figure 12 and

to table 5. The source generating the low-frequency jet noise component dominating in the downstream direction, which is probably located in this flow region,[55–58] is thus weakened. The use of a finer axial mesh in Jetv9ring1024dz appears fortunately to remove this numerical artifact, as indicated by the good agreement with acoustic measurements at low Strouhal numbers in this case.

V. Conclusion

In the present paper, results provided by five compressible LES of a round jet at Mach number 0.9 and Reynolds number 10^5 characterized by tripped nozzle-exit boundary layers are presented. They are found to vary in a negligible way with the tripping methodology, but significantly with the grid resolution. To obtain satisfactory jet features, it appears that the discretization should be very fine not only at the nozzle lip but also all along the shear-layer development. Mesh grids should also be nearly isotropic, which implies in particular to avoid coarse azimuthal discretization, as well as rapid grid stretching in the axial direction, so as to properly calculate turbulent structures up to the end of the jet potential core. In practice, mesh spacings Δr, $\Delta\theta$ and Δz lower than $\delta_\theta/2$, where δ_θ is the exit boundary-layer thickness, are recommended in cylindrical coordinates.

Regarding the physical relevance of the results obtained for the initially nominally turbulent jet at $\mathrm{Re}_D = 10^5$ considered in this study, the mean and turbulent flow fields from Jetv9ring1024dz simulation using 252 million grid points are in good agreement with experimental data for jets at Reynolds numbers higher than 5×10^5. This is particularly the case for the potential core length and for the downstream velocity decay. The increase of the turbulent intensities along the shear layer is also smooth, as expected in an initially turbulent jet. As for the radiated noise, a component associated with vortex pairings in the mixing layers is observed, yielding an additional hump in the sound spectra around 2 dB above the asymptotically low levels reached at very high Reynolds numbers. Further works will be carried out to support the present findings, and to describe turbulent mechanisms in tripped jets. The influence of the initial turbulence levels and of the Reynolds number could particularly be characterized.

Acknowledgments

This work was granted access to the HPC resources of the Institut du Développement et des Ressources en Informatique Scientifique (IDRIS) under the allocation 2010-020204 made by GENCI (Grand Equipement National de Calcul Intensif). The authors are especially grateful to Jean-Michel Dupays from IDRIS for his technical assistance. They would also like to thank Dr Khairul Zaman for his remarks on the present works.

References

[1]Batt, R.G., "Some measurements on the effect of tripping the two-dimensional shear layer," *AIAA J.*, Vol. 13, No. 2, 1975, pp. 245-247.

[2]Hill, W.G., Jenkins, R.C., and Gilbert, B.L., "Effects of the initial boundary-layer state on turbulent jet mixing," *AIAA J.*, Vol. 14, No. 11, 1976, pp. 1513-1514.

[3]Gutmark, E. and Ho, C.-M., "Preferred modes and the spreading rates of jets," *Phys. Fluids*, Vol. 26, No. 10, 1983, pp. 2932-2938.

[4]Raman, G., Zaman, K.B.M.Q., and Rice, E.J., "Initial turbulence effect on jet evolution with and without tonal excitation," *Phys. Fluids A*, Vol. 1, No. 7, 1989, pp. 1240-1248.

[5]Crighton, D.G., "Acoustics as a branch of fluid mechanics," *J. Fluid Mech.*, Vol. 106, 1981, pp. 261-298.

[6]Hussain, A.K.M.F., "Coherent structures–reality and myth," *Phys. Fluids*, Vol. 26, No. 10, 1983, pp. 2816-2850.

[7]Zaman, K.B.M.Q., "Far-field noise of a subsonic jet under controlled excitation," *J. Fluid Mech.*, Vol. 152, 1985, pp. 83-111.

[8]Hussain, A.K.M.F and Zedan, M.F., "Effects of the initial condition on the axisymmetric free shear layer: Effects of the initial momentum thickness," *Phys. Fluids*, Vol. 21, No. 7, 1978, pp. 1100-1112.

[9]Hussain, A.K.M.F. and Zedan, M.F., "Effects of the initial condition on the axisymmetric free shear layer: Effects of the initial fluctuation level," *Phys. Fluids*, Vol. 21, No. 9, 1978, pp. 1475-1481.

[10]Zaman, K.B.M.Q., "Effect of initial condition on subsonic jet noise," *AIAA J.*, Vol. 23, 1985, pp. 1370-1373.

[11]Bridges, J.E. and Hussain, A.K.M.F., "Roles of initial conditions and vortex pairing in jet noise," *J. Sound Vib.*, Vol. 117, No. 2, 1987, pp. 289-311.

[12]Grosche, F.-R., "Distributions of sound source intensities in subsonic and supersonic jets," AGARD-CP-131, 1974, pp. 4-1 to 4-10.

[13]Husain, Z.D. and Hussain, A.K.M.F., "Axisymmetric mixing layer: influence of the initial and boundary conditions," *AIAA J.*, Vol. 17, No. 1, 1979, pp. 48-55.

[14]Hussain, A.K.M.F. and Husain, Z.D., "Turbulence structure in the axisymmetric free mixing layer," *AIAA J.*, Vol. 18, No. 12, 1980, pp. 1462-1469.

[15]Lepicovsky, J. and Brown, W.H., "Effects of nozzle exit boundary-layer conditions on excitability of heated free jets," *AIAA J.*, Vol. 27, No. 6, 1989, pp. 712-718.

[16]Raman, G., Rice, E.J., and Reshotko, E., "Mode spectra of natural disturbances in a circular jet and the effect of acoustic forcing," *Exp. Fluids*, Vol. 17, 1994, pp. 415-426.

[17]Arakeri, V.H., Krothapalli, A., Siddavaram, V., Alkislar, M.B., and Lourenco, L., "On the use of microjets to suppress turbulence in a Mach 0.9 axisymmetric jet," *J. Fluid Mech.*, Vol. 490, 2003, pp. 75-98.

[18]Morris, P.J. and Zaman, K.B.M.Q., "Velocity measurements in jets with application to noise source modelling," *J. Sound Vib.*, Vol. 329, No. 4, 2009, pp. 394-414.

[19]Wygnanski, I., Oster, D., Fiedler, H., and Dziomba, B., "On the perseverance of a quasi-two-dimensional eddy-structure in a turbulent mixing layer," *J. Fluid Mech.*, Vol. 93, No. 2, 1979, pp. 325-335.

[20]Bell, J.H. and Mehta, R.D., "Development of a two-stream mixing layer from tripped and untripped boundary layers," *AIAA J.*, Vol. 28, No. 12, 1990, pp. 2034-2042.

[21]Strykowski, P.J. and Russ, S., "The effect of boundary-layer turbulence on mixing in heated jets," *Phys. Fluids A*, Vol. 4, No. 5, 1992, pp. 865-868.

[22]Russ, S. and Strykowski, P.J., "Turbulent structure and entrainment in heated jets: The effect of initial conditions," *Phys. Fluids A*, Vol. 5, No. 12, 1993, pp. 3216-3225.

[23]Maestrello, L. and McDaid, E., "Acoustic characteristics of a high-subsonic jet," *AIAA J.*, Vol. 9, No. 6, 1971, pp. 1058-1066.

[24]Antonia, R.A. and Zhao, Q., "Effect of initial conditions on a circular jet," *Exp. Fluids*, Vol. 31, 2001, pp. 319-323.

[25]Xu, G. and Antonia, R.A., "Effects of different initial conditions on a turbulent free jet," *Exp. Fluids*, Vol. 33, 2002, pp. 677-683.

[26]Colonius, T. and Lele, S.K., "Computational aeroacoustics: progress on nonlinear problems of sound generation," *Progress in Aerospace Sciences*, Vol. 40, 2004, pp. 345-416.

[27]Bogey, C. and Bailly, C., "Contributions of CAA to jet noise research and prediction," *Int. J. Comput. Fluid Dyn.*, Vol. 18, No. 6, 2004, pp. 481-491.

[28]Wang, M., Freund J.B., and Lele, S.K., "Computational prediction of flow-generated sound," *Annu. Rev. Fluid. Mech.*, Vol. 38, 2006, pp. 483-512.

[29]Freund, J.B., "Noise sources in a low-Reynolds-number turbulent jet at Mach 0.9," *J. Fluid Mech.*, Vol. 438, 2001, pp. 277-305.

[30]Stanley, S.A. and Sarkar, S., "Influence of nozzle conditions and discrete forcing on turbulent planar jets," *AIAA J.*, Vol. 38, No. 9, 2000, pp. 1615-1623.

[31]Bogey, C. and Bailly, C., "Effects of inflow conditions and forcing on a Mach 0.9 jet and its radiated noise," *AIAA J.*, Vol. 43, No. 5, 2005, pp. 1000-1007.

[32]Keiderling, F., Kleiser, L. and Bogey, C., "Numerical study of eigenmode forcing effects on jet flow development and noise generation mechanisms," *Phys. Fluids*, Vol. 21, No. 4, 2009, 045106.

[33]Kim, J. and Choi, H., "Large eddy simulation of a circular jet: effect of inflow conditions on the near field," *J. Fluid Mech.*, Vol. 620, 2009, pp. 383-411.

[34]Bogey, C. and Bailly, C., "Influence of nozzle-exit boundary-layer conditions on the flow and acoustic fields of initially laminar jets," submitted to *J. Fluid Mech.*, 2010. See also AIAA Paper 2009-3409, 2009.

[35]Bogey, C., Barré, S., and Bailly, C., "Direct computation of the noise generated by subsonic jets originating from a straight pipe nozzle," *Int. J. of Aeroacoustics*, Vol. 7, No. 1, 2008, pp. 1-22.

[36]Uzun, A. and Hussaini, M., "Investigation of high frequency noise generation in the near-nozzle region of a jet using large eddy simulation," *Theoret. Comput. Fluid Dynamics*, Vol. 21, No. 4, 2007, pp. 291-321.

[37]Mohseni, K. and Colonius, T., "Numerical treatment of polar coordinate singularities," *J. Comput. Phys.*, Vol. 157, No. 2, 2000, pp. 787-795.

[38]Bogey, C. and Bailly, C., "A family of low dispersive and low dissipative explicit schemes for flow and noise computations," *J. Comput. Phys.*, Vol. 194, No. 1, 2004, pp. 194-214.

[39]Bogey, C., de Cacqueray, N., and Bailly, C., "A shock-capturing methodology based on adaptative spatial filtering for high-order non-linear computations," *J. Comput. Phys.*, Vol. 228, No. 5, 2009, pp. 1447-1465.

[40]Berland, J., Bogey, C., Marsden, O., and Bailly, C., "High-order, low dispersive and low dissipative explicit schemes for multi-scale and boundary problems," *J. Comput. Phys.*, Vol. 224, No. 2, 2007, pp. 637-662.

[41]Bogey, C. and Bailly, C., "Large Eddy Simulations of transitional round jets: influence of the Reynolds number on flow development and energy dissipation," *Phys. Fluids*, Vol. 18, No. 6, 2006, 065101.

[42]Bogey, C. and Bailly, C., "Large eddy simulations of round jets using explicit filtering with/without dynamic Smagorinsky model," *Int. J. Heat and Fluid Flow*, Vol. 27, No. 4, 2006, pp. 603-610.

[43]Bogey, C. and Bailly, C., "Turbulence and energy budget in a self-preserving round jet: direct evaluation using large-eddy simulation," *J. Fluid Mech.*, Vol. 627, 2009.

[44]Tam, C.K.W and Dong, Z., "Radiation and outflow boundary conditions for direct computation of acoustic and flow disturbances in a nonuniform mean flow., *J. Comput. Acoust.*, Vol. 4, No. 2,, 1996, pp. 175201.

[45]Bogey, C. and C. Bailly, C., "Three-dimensional non reflective boundary conditions for acoustic simulations: far-field formulation and validation test cases," *Acta Acustica*, Vol. 88, No. 4, 2002, pp. 463-471.

[46]Bogey, C., Barré, S., Juvé, D., and Bailly, C., "Simulation of a hot coaxial jet : direct noise prediction and flow-acoustics correlations," *Phys. Fluids*, Vol. 21, No. 3, 2009, 035105.

[47]Davies, P.O.A.L., Fisher, M.J., and Barratt, M.J., "The characteristics of the turbulence in the mixing region of a round jet," *J. Fluid Mech.*, Vol. 15, 1963, pp. 337-367.

[48]Fleury, V., Bailly, C., Jondeau, E., Michard, M., and Juvé, D., "Space-time correlations in two subsonic jets using dual-PIV measurements," *AIAA J.*, Vol. 46, No. 10, 2008, pp. 2498-2509.

[49]Lau, J.C., Morris, P.J., and Fisher, M.J., "Measurements in subsonic and supersonic free jets using a laser velocimeter," *J. Fluid Mech.*, Vol. 93, No. 1, 1979, pp. 1-27.

[50]Ahuja, K.K., Tester, B.J., and Tanna, H.K., "Calculation of far field jet noise spectra from near field measurements with true source location," *J. Sound Vib.*, Vol. 116, No. 3, 1987, pp. 415-426.

[51]Mollo-Christensen, E., Kolpin, M.A., and Martucelli, J.R., "Experiments on jet flows and jet noise far-field spectra and directivity patterns," *J. Fluid Mech.*, Vol. 18, 1964, pp. 285-301.

[52]Lush, P.A., "Measurements of subsonic jet noise and comparison with theory," *J. Fluid Mech.*, Vol. 46, No. 3, 1971, pp. 477-500.

[53]Tanna, H.K., "An experimental study of jet noise. Part I: Turbulent mixing noise," *J. Sound Vib.*, Vol. 50, No. 3, 1977, pp. 405-428.

[54]Bogey, C., Barré, S., Fleury, V., Bailly, C., and Juvé, D., "Experimental study of the spectral properties of near-field and far-field jet noise," *Int. J. of Aeroacoustics*, Vol. 6, No. 2, 2007, pp. 73-92.

[55]Schaffar, M., "Direct measurements of the correlation between axial in-jet velocity fluctuations and far field noise near the axis of a cold jet," *J. Sound Vib.*, Vol. 64, No. 1, 1979, pp. 73-83.

[56]Panda, J., Seasholtz, R.G., and Elam, K.A., "Investigation of noise sources in high-speed jets via correlation measurements," *J. Fluid Mech.*, Vol. 537, 2005, pp. 349-385.

[57]Bogey, C. and Bailly, C., "An analysis of the correlations between the turbulent flow and the sound pressure field of subsonic jets," *J. Fluid Mech.*, Vol. 583, 2007, pp. 71-97.

[58]Tam, C.K.W., Viswanathan, K., Ahuja, K.K., and Panda, J., "The sources of jet noise: experimental evidence," *J. Fluid Mech.*, Vol. 615, 2008, p. 253-292.